AoI-Aware Joint Resource Allocation in Multi-UAV Aided Multi-Access Edge Computing Systems

Shuai Shen, Halvin Yang, Kun Yang, *Fellow, IEEE,* Kezhi Wang, *Senior Member, IEEE,* and Guopeng Zhang,

***Abstract*—Compared with traditional latency, age of information (AoI) is regarded as a more sufficient metric to measure the freshness of information. In this paper, we investigate the AoI-aware unmanned aerial vehicle (UAV) aided multi-access edge computing (MEC) system, where the UAVs, equipped with MEC servers, provide computing service to the ground IoT devices, which have heterogeneous average peak AoI (APAoI) requirements. According to the Poisson process model, the probabilistic LoS channel model and the M/D/1 queue model, the APAoI of each IoT device is derived, which involves the hovering locations of the UAVs and the communication and computing resources. Then, considering the APAoI requirements of the IoT devices, we formulate the energy consumption minimization problem, in which the offloading strategy and the transmit power of the devices, and the communication and computing resources allocation as well as the hovering locations of the UAVs are jointly optimized. The formulated optimization problem is non-convex. To efficiently solve it, we decompose it into five subproblems and propose an alternative algorithm based on the traditional mathematical method, KKT conditions, and successive convex approximation technique. Extensive simulation results are provided to show the performance gain of the proposed algorithm.**

***Index Terms*—Age of information, unmanned aerial vehicle, multi-access edge computing, resource allocation.**

I. Introduction

THE unprecedented proliferation of Internet of Things (IoT) devices leads to the explosive growth in the number of computation-intensive and latency-sensitive applications, such as face recognition, automatic navigation, and virtual/augmented reality [1]. However, IoT devices are normally equipped with limited battery capacity and computing capability, which may not meet the requirements of these sophisticated applications. Although cloud computing can relieve the workload of IoT devices, the massive offloading data raises the load of the core network, thereby increasing the computing latency.

Multi-access edge computing (MEC) is regarded as a promising technology to alleviate the network congestion and improve the computation efficiency, through deploying computing resource at the edges of networks in proximity to IoT devices [2]. Usually, MEC servers are configured in the base stations (BSs) and access points (APs). By offloading the computing tasks to the nearby infrastructures, the round-trip latency and the energy consumption of the IoT devices can be effectively reduced [3]. However, the locations of these terrestrial infrastructures are fixed, and their coverage is limited. The quality of computing service can not be guaranteed in the scenarios with remote IoT devices or sparsely distributed infrastructures.

Fortunately, due to the high flexibility and maneuverability, unmanned aerial vehicles (UAVs) provide a solution to the above issues. Carrying MEC servers, UAVs can act as aerial computing platforms to provide resilient and reliable computing service for ground IoT devices [4]. The locations of UAVs can be configured according to the requirements of network applications. Through allocating the resource of UAVs reasonably, the system performance can be significantly improved. Owing to these exclusive characteristics, UAVs have been widely employed in various scenarios, such as environmental monitoring, traffic surveillance, and aerial imaging [5].

So far, the research on MEC systems mainly focuses on the latency caused by the communication, queuing, and computing. The latency of information refers to the time elapsed from the start of transmission to the completion of execution, which is not a sufficient measurement of freshness [6]. However, the freshness of the computing tasks' information is also crucial for the systems where the status updates must be disseminated timely, such as intelligent transportation and remote surgery systems [7]. To characterize the freshness of information, a new metric, called age of information (AoI), has been proposed [8], which is defined as the time elapsed since the generation of the latest processed computing task in MEC systems.

A. Related Work

As a key technology to provide efficient computing service for IoT devices, MEC has been extensively investigated. The main focuses are the energy efficiency [9] [10] and the latency [11] [12]. The research fields include vehicular edge computing systems [13] [14], wireless power transfer (WPT) enabled MEC systems [15] [16], and non-orthogonal multiple

This work was supported in part by Natural Science Foundation of China under Grant No. 62132004, and in part by Sichuan Science and Technology Program under Grant No. 22QYCX0168.

Shuai Shen is with the School of Information and Communication Engineering, University of Electronic Science and Technology of China, Chengdu 611731, China (e-mail: shuaishen@std.uestc.edu.cn).

Halvin Yang is with the Department of Electronic and Electrical Engineering, University College London (UCL), London, United Kingdom (e-mail: uceehhy@ucl.ac.uk).

Kun Yang (*Corresponding author*) is with the School of Computer Science and Electronic Engineering, University of Essex, Colchester CO4 3SQ, U.K, and also with the School of Information and Communication Engineering, University of Electronic Science and Technology of China, Chengdu 611731, China (e-mail: kunyang@essex.ac.uk).

Kezhi Wang is with Department of Computer Science, Brunel University London, Uxbridge, Middlesex, UB8 3PH (email: kezhi.wang@brunel.ac.uk).

Guopeng Zhang is with the School of Computer Science and Technology, China University of Mining and Technology, Xuzhou 221116, China (email: gpzhang@cumt.edu.cn).

access based MEC systems [17], etc. Given the paramount significance of communication and computing resources in MEC systems, prior literature has predominantly focused on the joint allocation of these resources.

Due to the advantage of flexibility and mobility, the configuration of UAVs is more on-demand and diverse compared with the fixed infrastructures. Since UAVs can efficiently improve IoT devices' quality of the experience, the UAV-aided MEC systems have attracted much attention. However, restricted by the battery capacity of UAVs and IoT devices, the energy efficiency is still a challenge for UAV-aided MEC systems. In [18], Pervez *et al.* proposed an optimization framework to minimize the energy consumption and latency in a multi-UAV aided MEC system under time-varying channel. Considering the channel uncertainty, Mao *et al.* investigated the robust and secure task transmission and computation scheme in multi-antenna UAV-assisted MEC networks, where the UAV is empowered with MEC and relay functions [19]. In [20], Dai *et al.* studied the energy-efficient scheduling in a UAV-and-BS hybrid enabled MEC system where the computing tasks can be executed locally, offloaded to the UAVs directly or the BS indirectly. By integrating WPT into traditional systems, Hu *et al.* proposed a wireless-powered UAV-assisted MEC architecture to support the energy consumption of MEC, in which the UAV functions as a MEC server and an information and energy relay [21].

In the field of UAV-aided systems, the latency is commonly regarded as the metric [22]–[25]. However, traditional latency methods are insufficient to measure the recency of data received. As a more precise metric, the concept of AoI is proposed to characterize the freshness of information. It has been exploited in many fields, such as vehicular networks [26] [27], WPT enabled networks [28] [29], and UAV-assisted networks [30] [31], etc. In MEC networks, AoI has also raised a lot of attention. In [32], Ning *et al.* designed a MEC-enabled health monitoring system and minimized the system cost which relies on the medical criticality, AoI and energy consumption. Considering the random energy arrivals, heterogeneous harvesting modes, and the stochastic transmission and computing process, Liu *et al.* investigated an AoI minimization problem in MEC-assisted WPT-enabled networks and proposed an online age-aware status update scheme [33]. To guarantee the fair access and low AoI, Wu *et al.* proposed a multi-objective optimization scheme for MEC-assisted vehicle-to-infrastructure networks [34]. However, there are few researches on the AoI-aware UAV-aided MEC networks at present. In [35], Qin *et al.* investigated the AoI-aware scheduling for air-ground collaborative MEC networks to minimize the weighted AoI of users, considering the computing resource and the UAV's energy constraints. To address the security issues in UAV-aided MEC networks, Wang *et al.* studied an channel access-based AoI optimization problem under channel access attacks with a game theory viewpoint [36]. In [37], Han *et al.* developed a UAV-aided intelligent transportation system and minimized the average peak AoI by optimizing the deployment of UAVs.

In summary, there exists extensive researches on the latency-oriented UAV-aided MEC networks, but few on the AoI-aware ones. The rare literature predominantly aims at minimizing AoI, often overlooking the fact that AoI merely requires staying below an acceptable threshold. Excessive reduction in AoI may increase the burden on systems. Additionally, the majority of the existing works regard the computing resource as a fixed entity. Only the authors in [35] considered the impact of the computing resource allocation on AoI. However, they ignored the influence of the communication resource. In practical systems, AoI relies on both the communication and computing resources. To the best of our knowledge, there is still no work studying the jointly optimization of the hovering locations of UAVs, the communication and computing resources in the AoI-aware UAV-aided MEC system.

B. Our Contribution

Different from the above work, we regard the AoI metric as a requirement of the IoT device. The average peak AoI (APAoI) of the devices can not exceed their requirements. In this paper, we aim to minimize the total energy consumption of the UAVs and the IoT devices for processing the tasks generated in unit time by jointly optimizing the offloading strategy and the transmit power of the devices, and the bandwidth and computing resource allocation as well as the hovering locations of the UAVs, subject to the APAoI, the communication and computing constraints. The main contributions of this paper are summarized as follows.

1) Based on the Poisson process model of the task generation, the probabilistic LoS channel model of the ground-UAV links and the M/D/1 queue model, we derive the mathematical expression of the APAoI for each IoT device.
2) Considering the practical scenario, we treat the APAoI of each IoT device as a constraint rather than an objective. In the constraint, the offloading strategy, the transmit power and the channel bandwidth of the devices, as well as the computing resource and the hovering locations of the UAVs are all included.
3) With the heterogeneous APAoI requirements of the IoT devices, we formulate the energy consumption minimization problem. This is a non-convex optimization problem, which is difficult to solve directly. To efficiently obtain the high-quality solution, we decompose the optimization problem into five subproblems: the offloading strategy, the transmit power, the frequency bandwidth, the computing resource and the hovering location optimization problems. The first and the last subproblems are still non-convex. We solve them through successive convex approximation (SCA) technique. For the second subproblem, it is solved by the traditional mathematical method. The third and the fourth subproblems are convex optimization problems, and thus we derive their solutions through the interoir-point method and the KKT conditions, respectively. Finally, by combining the solutions of these subproblems, we propose an alternative algorithm.

The reminder of this paper is organized as follows. In Section II, the AoI-aware UAV-aided MEC system model is presented and the energy consumption minimization problem is formulated. The proposed algorithm is presented in Section

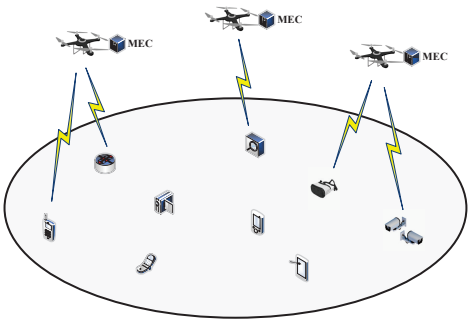

Fig. 1. AoI-aware UAV-aided MEC system.

III. Section IV provides numerical results to analyze the features of the system, and certify the performance of the proposed algorithm. The conclusion is drawn in Section V.

II. System Model and Problem Formulation

In this section, we first introduce the AoI-aware UAV-aided MEC system model. Then, the energy consumption minimization problem is formulated.

A. System Model

As shown in Fig. 1, consider a multi-UAV aided MEC system with K UAVs and M ground IoT devices. Each UAV carries a MEC server to provide computing service for the IoT devices. The set of the UAVs and the devices are denoted as $\mathcal{K}$ and $\mathcal{M}$, respectively, and thus the cardinalities of them are $|\mathcal{K}| = K$ and $|\mathcal{M}| = M$. Without loss of generality, the locations of the UAVs and the IoT devices are represented by the three-dimensional (3D) Cartesian coordinates $\mathbf{q}_k = [x_k, y_k, z_k]^T \in \mathbb{R}^{3\times 1}$ and $\mathbf{w}_m = [x_m, y_m, 0]^T \in \mathbb{R}^{3\times 1}$, respectively. We assume that different IoT devices have different types of computing tasks, and the tasks generated by one device are the same. Denote D_m as the data size of each computing task generated by the m-th IoT device, and $F_m = C_m D_m$ as the number of CPU cycles required to execute the task, where C_m (in cycle/bit) represents the number of CPU cycles for computing 1 bit data offloaded from the m-th IoT device. The computing task generation of each device can be modeled as a Poisson process with the generation rate λ_m independently. It is assumed that once the tasks are generated, the devices transmit them to the UAV immediately. Hence, the arrival of each device's tasks at the UAV is also a Poisson process with arrival rate λ_m.

B. Communication Model

We adopt the probabilistic LoS channel model for the ground-air links [38], where the channel is modeled as a combination of LoS and NLoS links. The occurrence probability of LoS link depends on the elevation angle and the propagation environment. Assuming that the antennas on the UAVs and the IoT devices are placed vertically, the LoS probability is given by

$$P_{m,k}^{LoS} = \frac{1}{1 + a\exp(-b[\theta_{m,k} - a])}, \tag{1}$$

where a and b are the constants determined by the environment, and $\theta_{m,k} = \frac{180}{\pi}\arcsin(\frac{z_k}{d_{m,k}})$ is the elevation angle between the m-th IoT device and the k-th UAV, with $d_{m,k} = \|\mathbf{q}_k - \mathbf{w_m}\|$ denoting the distance between them. Then, the NLoS probability is obtained as $P_{m,k}^{NLoS} = 1 - P_{m,k}^{LoS}$.

The LoS and NLoS channel power gain between the m-th IoT device and the k-th UAV are respectively given by [39]

$$h_{m,k}^{LoS} = \rho_0 d_{m,k}^{-\alpha_L}, h_{m,k}^{NLoS} = \kappa\rho_0 d_{m,k}^{-\alpha_N}, \tag{2}$$

where ρ_0 is the path loss at the reference distance $d_0 = 1m$, $\kappa < 1$ is the additional attenuation factor due to the NLoS propagation, α_L and α_N are the LoS and NLoS path loss exponents respectively. Then, the achievable rate between the m-th IoT device and k-th UAV under the LoS and NLoS states can be respectively expressed as

$$\begin{aligned} R_{m,k}^{LoS} &= B_{m,k}\log_2(1 + \frac{p_m h_{m,k}^{LoS}}{B_{m,k}N_0}) \\ &= B_{m,k}\log_2(1 + \frac{p_m\gamma}{B_{m,k}d_{m,k}^{\alpha_L}}), \end{aligned} \tag{3}$$

$$\begin{aligned} R_{m,k}^{NLoS} &= B_{m,k}\log_2(1 + \frac{p_m h_{m,k}^{NLoS}}{B_{m,k}N_0}) \\ &= B_{m,k}\log_2(1 + \frac{\kappa p_m\gamma}{B_{m,k}d_{m,k}^{\alpha_N}}), \end{aligned} \tag{4}$$

where $B_{m,k}$ is the channel bandwidth that k-th UAV allocates to the m-th IoT device, p_m is the transmit power of the m-th IoT device, and $\gamma = \frac{\rho_0}{N_0}$ with N_0 representing the power spectral density of the additive white Gaussian noise (AWGN) at the receiver. As a result, the expected rate between the m-th IoT device and k-th UAV can be expressed as

$$\bar{R}_{m,k} = \mathbb{E}[R_{m,k}] = P_{m,k}^{LoS}R_{m,k}^{LoS} + P_{m,k}^{NLoS}R_{m,k}^{NLoS}. \tag{5}$$

It is assumed that each computing task offloaded from one IoT device can be partitioned into several smaller-size tasks that can be separately offloaded to multiple UAVs, and executed in parallel [40]. The offloading strategy of the m-th IoT device is denoted as $a_{m,k}$, which represents the proportion of each task offloaded from the m-th IoT device to the k-th UAV. Therefore, the duration for the m-th IoT device to offload one computing task to the k-th UAV is

$$T_{m,k}^{O} = \frac{a_{m,k}D_m}{\bar{R}_{m,k}}. \tag{6}$$

Then, the energy consumed by the m-th IoT device to offload a task to the k-th UAV can be obtained as

$$E_{m,k}^{O} = p_m\frac{a_{m,k}D_m}{\bar{R}_{m,k}}. \tag{7}$$

C. Computing Model

The procedure of task execution consists of three parts: offloading, queuing, and computing, as shown in Fig. 2. In the offloading part, the IoT devices are assumed to transmit data in non-overlapping frequency bands through frequency division multiple access (FDMA). It is also assumed that the UAV cache is divided into M sub-caches, each serving as a queue for a type of task, i.e., an IoT device. Therefore, in

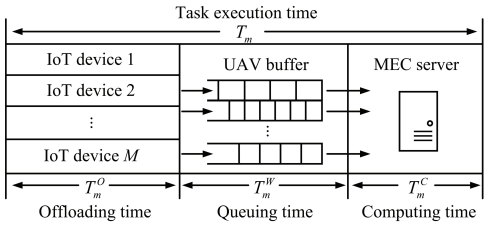

Fig. 2. Workflow of task offloading.

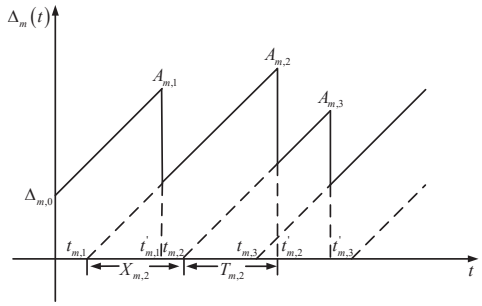

Fig. 3. AoI of the m-th IoT device.

the queuing part, the tasks of each IoT device are temporarily stored in its queue, then executed under first-come-first-served (FCFS) discipline. Denoting $f_{m,k}$ as the CPU frequency (in Hz) used by the k-th UAV to execute the tasks offloaded from the m-th IoT device, the computing duration can be expressed as

$$T_{m,k}^C = \frac{a_{m,k} F_m}{f_{m,k}}. \tag{8}$$

Then, the energy consumption of the k-th UAV for executing a task of the m-th IoT device can be obtained as

$$E_{m,k}^C = \eta a_{m,k} F_m f_{m,k}^2, \tag{9}$$

where η denotes the effective switched capacitance.

As for the computing part, the MEC server processes the tasks received from different queues simultaneously. Under this workflow, given the transmit rate and computing resource allocation, the offloading and the computing duration of each task are deterministic. Hence, this is an M/D/1 queue model, in which the average waiting time of the tasks generated by the m-th IoT device is given by

$$T_{m,k}^W = \frac{\lambda_m}{2\frac{f_{m,k}}{a_{m,k}F_m}\left(\frac{f_{m,k}}{a_{m,k}F_m} - \lambda_m\right)}. \tag{10}$$

D. AoI Model

AoI is a metric that measures the freshness of the information generated by the IoT devices. The AoI of the m-th IoT device at time t can be given by

$$\Delta_m(t) = t - \delta_m(t), \tag{11}$$

where $\delta_m(t)$ denotes the time when the latest executed task of the m-th IoT device is generated. As shown in Fig. 3, we denote $t_{m,n}$ and $t'_{m,n}$ as the times that the n-th task of the m-th IoT device is generated and executed, respectively[1]. Then, the inter-generation time between two consecutive tasks of the m-th IoT device can be expressed as

$$X_{m,n} = t_{m,n} - t_{m,n-1}, \tag{12}$$

and the processing duration for the n-th task of the m-th IoT device can be expressed as

$$T_{m,n} = t'_{m,n} - t_{m,n}. \tag{13}$$

Since the task generation of the m-th IoT device is modeled as a Poisson process with rate λ_m, its task generation interval $X_{m,n}$ is an independent and identically distributed (i.d.d.) exponential random variable with $\mathbb{E}[X_{m,n}] = 1/\lambda_m$. Moreover, as mentioned in Section II-C, the execution duration is composed of three parts. Therefore, the average execution duration for the tasks of the m-th IoT device can be expressed as $\mathbb{E}[T_{m,n}] = \max\{T_{m,k}^O + T_{m,k}^W + T_{m,k}^C, \forall m \in \mathcal{M}, \forall k \in \mathcal{K}\}$.

The peak AoI is the AoI when the execution of a task is completed. Observing from Fig. 3, the peak AoI of the n-th task from the m-th IoT device can be derived as

$$A_{m,n} = X_{m,n} + T_{m,n}. \tag{14}$$

Then, the APAoI of the m-th IoT device can be obtained as

$$\begin{aligned}\Gamma_m &= \lim_{N\to\infty} \frac{1}{N} \sum_{n=1}^{N} A_{m,n} = \mathbb{E}[A_{m,n}] \\ &= \mathbb{E}[X_{m,n}] + \mathbb{E}[T_{m,n}].\end{aligned} \tag{15}$$

E. Problem Formulation

We aim to minimize the total energy consumption of the system for executing the tasks generated in unit time by jointly optimizing the offloading strategy $\mathbf{A} = \{a_{m,k}, \forall m \in \mathcal{M}, \forall k \in \mathcal{K}\}$, the transmit power $\mathbf{P} = \{p_m, \forall m \in \mathcal{M}\}$, the frequency bandwidth $\mathbf{B} = \{B_{m,k}, \forall m \in \mathcal{M}, \forall k \in \mathcal{K}\}$, the computing resource $\mathbf{F} = \{f_{m,k}, \forall m \in \mathcal{M}, \forall k \in \mathcal{K}\}$, and the hovering location $\mathbf{Q} = \{\mathbf{q}_k, \forall k \in \mathcal{K}\}$. The optimization problem is

[1]The n-th task is one of the tasks generated by m-th IoT device. Since one device generates only one type of task, the data size of the tasks generated by one device are the same. Therefore, the size of the n-th task of the m-th IoT device is D_m.

formulated as

$$\min_{\mathbf{A},\mathbf{P},\mathbf{B},\mathbf{F},\mathbf{Q}} \sum_{m=1}^{M}\sum_{k=1}^{K}(E_{m,k}^{C}+E_{m,k}^{O}) \tag{16}$$

$$\text{s.t. } \mathbf{q}_{min} \le \mathbf{q}_k \le \mathbf{q}_{max}, \forall k \in \mathcal{K}, \tag{16a}$$

$$\|\mathbf{q}_k - \mathbf{q}_j\|^2 \ge d_{min}^2, \forall k \in \mathcal{K}, j \ne k, \tag{16b}$$

$$0 \le a_{m,k} \le 1, \forall m \in \mathcal{M}, \forall k \in \mathcal{K}, \tag{16c}$$

$$\sum_{k=1}^{K} a_{m,k} \ge 1, \forall m \in \mathcal{M}, \tag{16d}$$

$$f_{m,k} \ge \lambda_m a_{m,k} F_m, \forall m \in \mathcal{M}, \forall k \in \mathcal{K}, \tag{16e}$$

$$\sum_{m=1}^{M} f_{m,k} \le f_{max}, \forall k \in \mathcal{K}, \tag{16f}$$

$$B_{m,k} \ge 0, \forall m \in \mathcal{M}, \forall k \in \mathcal{K}, \tag{16g}$$

$$\sum_{m=1}^{M} B_{m,k} \le B_{max}, \forall k \in \mathcal{K}, \tag{16h}$$

$$0 \le p_m \le P_{max}, \forall m \in \mathcal{M}, \tag{16i}$$

$$\Gamma_m \le \tau_m, \forall m \in \mathcal{M}, \tag{16j}$$

where constraint (16a) restricts the hovering range of the UAVs with $\mathbf{q}_{min} = [x_{min}, y_{min}, z_{min}]^T \in \mathbb{R}^{3\times 1}$ and $\mathbf{q}_{max} = [x_{max}, y_{max}, z_{max}]^T \in \mathbb{R}^{3\times 1}$, constraint (16b) is the collision avoidance constraint with d_{min} denoting the minimum inter-UAV distance, constraint (16d) ensures that the computing tasks of each device are completely offloaded, constraint (16e) is the queue stability constraint that guarantees a finite queue, constraints (16f), (16h) and (16i) ensure that the allocation of the computing resource, frequency bandwidth and transmit power can not exceed their maximum value, with f_{max}, B_{max} and P_{max} representing the maximum CPU frequency, channel bandwidth and transmit power, respectively, and constraint (16j) is the APAoI tolerance constraint which limits the APAoI of each IoT device below their maximum tolerance, with τ_m denoting the APAoI requirement of the m-th IoT device.

Note that problem (16) is a non-convex optimization problem, which is difficult to obtain the optimal solution efficiently due to the non-convexity of $\bar{R}_m$. To tackle this difficulty, in the following, we propose an alternative algorithm to obtain a high-quality solution.

III. Proposed Solution to Problem (16)

Since the achievable rates under LoS and NLoS states are coupled through the LoS probability in (5), $\bar{R}_{m,k}$ is a highly complicated function with respect to the hovering locations. However, the NLoS component is much smaller than the LoS component in $\bar{R}_{m,k}$, due to the additional attenuation factor κ and the larger path loss exponent α_N [41]. To tackle the complicated $\bar{R}_{m,k}$ and guarantee the completion of the computing tasks, we approximate the expected rate to its lower bound as [41], which is given by

$$\bar{R}_{m,k} \ge P_{m,k}^{LoS} R_{m,k}^{LoS} = \hat{R}_{m,k}. \tag{17}$$

Then, problem (16) is transformed into

$$\min_{\mathbf{A},\mathbf{P},\mathbf{B},\mathbf{F},\mathbf{Q}} \sum_{m=1}^{M}\sum_{k=1}^{K}(E_{m,k}^{C}+\hat{E}_{m,k}^{O}) \tag{18}$$

$$\text{s.t. (16a)} - \text{(16i)},$$

$$\hat{\Gamma}_m \le \tau_m, \forall m \in \mathcal{M}, \tag{18a}$$

where $\hat{E}_{m,k}^{O} = p_m \frac{a_{m,k} D_m}{\hat{R}_{m,k}}$ and $\hat{\Gamma}_m = \frac{1}{\lambda_m} + \max\{\hat{T}_{m,k}^{O} + T_{m,k}^{W} + T_{m,k}^{C}, \forall k \in \mathcal{K}\}$ with $\hat{T}_{m,k}^{O} = \frac{a_{m,k} D_m}{\hat{R}_{m,k}}$.

Then, due to the existence of the maximum function $\max\{\cdot\}$ in constraint (18a), problem (18) is difficult to solve. To address this issue, we further transform the problem into a more tractable form as follows.

$$\min_{\mathbf{P},\mathbf{B},\mathbf{F},\mathbf{Q}} \sum_{m=1}^{M}\sum_{k=1}^{K}(E_{m,k}^{C}+\hat{E}_{m,k}^{O}) \tag{19}$$

$$\text{s.t. (16a)} - \text{(16i)},$$

$$\Phi_{m,k} \le \tau_m, \forall m \in \mathcal{M}, \forall k \in \mathcal{K}, \tag{19a}$$

where $\Phi_{m,k} = 1/\lambda_m + \hat{T}_{m,k}^{O} + T_{m,k}^{W} + T_{m,k}^{C}$. It is noted that problem (19) is still a non-convex problem. To solve it efficiently, we decompose problem (19) into five subproblems: the offloading strategy, the transmit power, the frequency bandwidth, the computing resource, and the hovering location optimization problems.

A. Offloading Strategy Optimization

Given any feasible transmit power $\mathbf{P}$, frequency bandwidth $\mathbf{B}$, computing resource $\mathbf{F}$, and hovering location $\mathbf{Q}$, problem (19) is transformed into

$$\min_{\mathbf{A}} \sum_{m=1}^{M}\sum_{k=1}^{K}(E_{m,k}^{C}+\hat{E}_{m,k}^{O}) \tag{20}$$

$$\text{s.t. (16c)} - \text{(16e)}, \text{(19a)}.$$

To address the non-convexity of the constraint (19a), we introduce the slack variable $\mathbf{X} = \{\chi_{m,k}, \forall m \in \mathcal{M}, \forall k \in \mathcal{K}\}$. Then, problem (20) is transformed into

$$\min_{\mathbf{A},\mathbf{X}} \sum_{m=1}^{M}\sum_{k=1}^{K}(E_{m,k}^{C}+\hat{E}_{m,k}^{O}) \tag{21}$$

$$\text{s.t. (16c)} - \text{(16e)},$$

$$\frac{1}{\lambda_m} + \hat{T}_{m,k}^{O} + \frac{\lambda_m}{2\chi_{m,k}} + T_{m,k}^{C} \le \tau_m, \forall m \in \mathcal{M}, \forall k \in \mathcal{K}, \tag{21a}$$

$$\chi_{m,k} \le \frac{f_{m,k}}{a_{m,k}F_m}\left(\frac{f_{m,k}}{a_{m,k}F_m} - \lambda_m\right), \forall m \in \mathcal{M}, \forall k \in \mathcal{K}. \tag{21b}$$

However, constraint (21b) is still non-convex. To address this issue, SCA technique is adopted to approximate the right-hand-side (RHS) of the inequality in constraint (21b) by a more tractable function at a given local point in each iteration.

It can be verified that the RHS of the inequality in constraint (21b) is convex with respective to $a_{m,k}$. Since any convex function is globally lower-bounded by its first-order Taylor

expansion at any given local point, its lower bound with given local point $a_{m,k}^r$ in the r-th iteration can be expressed as

$$\frac{f_{m,k}}{a_{m,k}F_m}(\frac{f_{m,k}}{a_{m,k}F_m}-\lambda_m)\geq \Lambda_{m,k}^r+\Omega_{m,k}^r(a_{m,k}-a_{m,k}^r), \tag{22}$$

where $\Lambda_{m,k}^r = \frac{f_{m,k}}{a_{m,k}^r F_m}(\frac{f_{m,k}}{a_{m,k}^r F_m}-\lambda_m)$ and $\Omega_{m,k}^r = \frac{f_{m,k}(\lambda_m F_m a_{m,k}^r - 2f_{m,k})}{F_m^2 (a_{m,k}^r)^3}$ are constants.

With any given local point $a_{m,k}^r$ and the lower bound expression in formula (22), problem (21) is approximated as

$$\min_{\mathbf{A},\mathbf{X}} \sum_{m=1}^{M}\sum_{k=1}^{K} O_{m,k}a_{m,k} \tag{23}$$
$$\text{s.t. (16c)} - \text{(16e)},$$
$$\frac{1}{\lambda_m}+\Upsilon_{m,k}a_{m,k}+\frac{\lambda_m}{2\chi_{m,k}}\leq \tau_m,$$
$$\forall m\in\mathcal{M},\forall k\in\mathcal{K}, \tag{23a}$$
$$\chi_{m,k}\leq \Lambda_{m,k}^r+\Omega_{m,k}^r(a_{m,k}-a_{m,k}^r),$$
$$\forall m\in\mathcal{M},\forall k\in\mathcal{K}, \tag{23b}$$

where $O_{m,k}=\frac{p_m D_m}{R_{m,k}}+\eta F_m f_{m,k}^2$ and $\Upsilon_{m,k}=\frac{D_m}{R_{m,k}}+\frac{F_m}{f_{m,k}}$ are constants. Note that the objective function and constraints (16c), (16d), (16e) and (23b) are linear, and constraint (23a) is convex. Therefore, problem (23) is convex, which can be solved by standard optimization method, such as the interior-point method.

B. Transmit Power Optimization

Given any feasible offloading strategy $\mathbf{A}$, frequency bandwidth $\mathbf{B}$, computing resource $\mathbf{F}$, and hovering location $\mathbf{Q}$, problem (19) is transformed into

$$\min_{\mathbf{P}} \sum_{m=1}^{M}\sum_{k=1}^{K} \hat{E}_{m,k}^O \tag{24}$$
$$\text{s.t. } G_{m,k}\leq p_m\leq P_{max},\forall m\in\mathcal{M},\forall k\in\mathcal{K}, \tag{24a}$$

where $G_{m,k} = \left(2^{H_{m,k}}-1\right)B_{m,k}d_{m,k}^{\alpha_L}/\gamma$, with $H_{m,k} = \frac{a_{m,k}D_m}{B_{m,k}P_{m,k}^{LoS}(\tau_m-\frac{1}{\lambda_m}-T_{m,k}^W-T_{m,k}^C)}$ being positive constant. Furthermore, we have the following lemma.

Lemma 1: The objective function is monotonically increasing with respect to p_m.

Proof: Please refer to Appendix A. ■

Based on Lemma 1, the solution of problem (24) can be obtained at the minimum transmit power $C_{m,k}$ that satisfies constraint (24a). Otherwise, p_m can always be decreased to decrease the objective value. Therefore, the solution can be expressed as

$$p_m^* = \max\left\{C_{m,k},\forall k\in\mathcal{K}\right\}. \tag{25}$$

C. Frequency bandwidth Optimization

With any given feasible offloading strategy $\mathbf{A}$, transmit power $\mathbf{P}$, computing resource $\mathbf{F}$, and hovering location $\mathbf{Q}$, problem (19) is transformed into

$$\min_{\mathbf{B}} \sum_{m=1}^{M}\sum_{k=1}^{K} \hat{E}_{m,k}^O \tag{26}$$
$$\text{s.t. (16g), (16h), (19a).}$$

It can be verified that this is a convex optimization problem, which can be solved by standard method, such as the interior-point method.

Remark 1: The bandwidth of each UAV is entirely allocated to the IoT devices. With the increase in frequency bandwidth, the energy consumption gradually decreases and approaches an asymptotic constant.

Proof: Please refer to Appendix B. ■

D. Computing resource Optimization

With any given feasible offloading strategy $\mathbf{A}$, transmit power $\mathbf{P}$, frequency bandwidth $\mathbf{B}$, and hovering location $\mathbf{Q}$, problem (19) is transformed into

$$\min_{\mathbf{F}} \sum_{m=1}^{M}\sum_{k=1}^{K} E_{m,k}^C \tag{27}$$
$$\text{s.t. (16e), (16f), (19a).}$$

It can be verified that this is a convex optimization problem. The solution of this problem can be obtained through KKT conditions as follows.

$$f_{m,k}^* = \frac{[(J_{m,k}\lambda_m+1)+\sqrt{J_{m,k}^2\lambda_m^2+1}]a_{m,k}F_m}{2J_{m,k}}, \tag{28}$$

where $J_{m,k}=\tau_m-\frac{1}{\lambda_m}-\hat{T}_{m,k}^O$ is a positive constant.

Proof: Please refer to Appendix C. ■

E. Hovering location Optimization

With any given feasible offloading strategy $\mathbf{A}$, transmit power $\mathbf{P}$, frequency bandwidth $\mathbf{B}$, and computing resource $\mathbf{F}$, problem (19) is transformed into

$$\min_{\mathbf{Q}} \sum_{m=1}^{M}\sum_{k=1}^{K} \hat{E}_{m,k}^O \tag{29}$$
$$\text{s.t. (16a), (16b), (19a).}$$

Note that this problem is still non-convex due to the coupling between the horizontal and vertical coordinates of the hovering location. Therefore, we further decompose problem (29) into the horizontal and vertical coordinate optimization problems.

1) Horizontal coordinate optimization problem: Given any feasible vertical coordinate z_k, problem (29) is transformed into

$$\min_{\mathbf{q}_k^h} \sum_{m=1}^{M}\sum_{k=1}^{K} \hat{E}_{m,k}^{O} \tag{30}$$
$$\text{s.t. (19a)},$$
$$\mathbf{q}_{min}^h \le \mathbf{q}_k^h \le \mathbf{q}_{max}^h, \forall k \in \mathcal{K}, \tag{30a}$$
$$\|\mathbf{q}_k^h - \mathbf{q}_j^h\|^2 \ge D^h, \forall k \in \mathcal{K}, j \ne k, \tag{30b}$$

where $\mathbf{q}_k^h = [x_k, y_k]^T \in \mathbb{R}^{2\times 1}$ denotes the horizontal coordinate of the k-th UAV's location, $\mathbf{q}_{min}^h = [x_{min}, y_{min}]^T \in \mathbb{R}^{2\times 1}$ and $\mathbf{q}_{max}^h = [x_{max}, y_{max}]^T \in \mathbb{R}^{2\times 1}$ denote the horizontal hovering range, and $D^h = d_{min}^2 - (z_k - z_j)^2$ is constant. Then, we introduce slack variables $\mu_{m,k}$ and $\theta_{m,k}$, $\forall m \in \mathcal{M}$, $\forall k \in \mathcal{K}$, and thus problem (30) is transformed into

$$\min_{\mathbf{q}_k^h, \mu_{m,k}, \theta_{m,k}} \sum_{m=1}^{M}\sum_{k=1}^{K} p_m \frac{a_{m,k} D_m}{\mu_{m,k}} \tag{31}$$
$$\text{s.t. (30a), (30b)},$$
$$\frac{a_{m,k} D_m}{\mu_{m,k}} \le S_{m,k}, \forall m \in \mathcal{M}, \forall k \in \mathcal{K}, \tag{31a}$$
$$\mu_{m,k} \le \hat{R}_{m,k}, \forall m \in \mathcal{M}, \forall k \in \mathcal{K}, \tag{31b}$$
$$\theta_{m,k} \le \frac{180}{\pi} \arcsin(\frac{z_k}{d_{m,k}}),$$
$$\forall m \in \mathcal{M}, \forall k \in \mathcal{K}, \tag{31c}$$

where $S_{m,k} = \tau_m - \frac{1}{\lambda_m} - T_{m,k}^W - T_{m,k}^C$. It can be verified that the objective function of problem (31) and $\hat{R}_{m,k}$ are monotonically decreasing and increasing with respect to $\mu_{m,k}$ and $\theta_{m,k}$, respectively. Therefore, at the optimal solution of problem (31), the constraints (31b) and (31c) can be met with equality, otherwise the objective value of problem (31) can always be decreased by increasing $\theta_{m,k}$ and $\mu_{m,k}$. Therefore, solving problem (31) is equivalent to solving problem (30).

In problem (31), constraints (30b), (31b) and (31c) are still non-convex due to the non-convexity of $\hat{R}_{m,k}$ and $\frac{180}{\pi}\arcsin(\frac{z_k}{d_{m,k}})$. To address this issue, SCA technique is adopted to approximate them respectively by a more tractable function at a given local point in each iteration.

It can be verified that the left-hand-side (LHS) of constraint (30b) is convex with respect to $\mathbf{q}_k^h$ and $\mathbf{q}_j^h$, which is globally lower-bounded by its first-order Taylor expansion at any given local point. Therefore, its lower bound at the given local points $\mathbf{q}_k^{h,r}$ and $\mathbf{q}_j^{h,r}$ in the r-th iteration can be given by

$$\|\mathbf{q}_k^h - \mathbf{q}_j^h\|^2 \ge -\|\mathbf{q}_k^{h,r} - \mathbf{q}_j^{h,r}\|^2 + 2(\mathbf{q}_k^{h,r} - \mathbf{q}_j^{h,r})^T(\mathbf{q}_k^h - \mathbf{q}_j^h) = d_{k,j}^{h,lb}. \tag{32}$$

To address the non-convexity of constraint (31b), we first introduce a lemma as follows.

Lemma 2: Given $A_1 \ge 0$ and $A_2 \ge 0$, $\psi(t_1, t_2) = \frac{A_1}{t_1}\log_2(1 + \frac{A_2}{t_2})$ is a convex function for $t_1 > 0$ and $t_2 > 0$.

Proof: Please refer to Appendix D. ■

Based on Lemma 2, it can be verified that $\hat{R}_{m,k}$ is a convex function with respect to $1 + a\exp(-b[\theta_{m,k} - a])$ and $d_{m,k}^{\alpha_L}$. Hence, the lower bound of $\hat{R}_{m,k}$ at the given local point $\mathbf{q}_k^{h,r} = [x_k^r, y_k^r]^T \in \mathbb{R}^{2\times 1}$ and $\theta_{m,k}^r$ in the r-th iteration can be expressed as

$$\begin{aligned}\hat{R}_{m,k} \ge & \hat{R}_{m,k}^r - V_{m,k}^r(d_{m,k}^{\alpha_L} - (d_{m,k}^r)^{\alpha_L}) \\ & - I_{m,k}^r a(\exp(-b[\theta_{m,k} - a]) - \exp(-b[\theta_{m,k}^r - a])) \\ = & \hat{R}_{m,k}^{lb},\end{aligned} \tag{33}$$

where $d_{m,k}^r = \|\mathbf{q}_k^{h,r} - \mathbf{w}_m\|$, $\hat{R}_{m,k}^r = \frac{B_{m,k}}{1+a\exp(-b[\theta_{m,k}-a])}\log_2(1 + \frac{p_m\gamma}{B_{m,k}(d_{m,k}^r)^{\alpha_L}})$, $I_{m,k}^r = \frac{B_{m,k}}{(1+a\exp(-b[\theta_{m,k}-a]))^2}\log_2(1 + \frac{p_m\gamma}{B_{m,k}(d_{m,k}^r)^{\alpha_L}})$, $V_{m,k}^r = \frac{B_{m,k}p_m\gamma}{\ln 2(1+a\exp(-b[\theta_{m,k}-a]))(d_{m,k}^r)^{\alpha_L}[B_{m,k}(d_{m,k}^r)^{\alpha_L} + p_m\gamma]}$ are positive constants.

Similarly, since the RHS of the inequality in constraint (31c) is convex with respect to $d_{m,k}$, its lower bound at the given local point $\mathbf{q}_k^{h,r}$ in the r-th iteration can be expressed as

$$\frac{180}{\pi}\arcsin(\frac{z_k}{d_{m,k}}) \ge Q_{m,k}^r - O_{m,k}^r(d_{m,k} - d_{m,k}^r), \tag{34}$$

where $Q_{m,k}^r = \frac{180}{\pi}\arcsin(\frac{z_k}{d_{m,k}^r})$, and $O_{m,k}^r = \frac{z_k}{(d_{m,k}^r)^2\sqrt{1 - \frac{z_k}{(d_{m,k}^r)^2}}}$ are positive constants.

According to the lower bounds expressions in (32), (33) and (34), with any given local points $\mathbf{q}_k^{h,r}$ and $\theta_{m,k}^r$, problem (31) can be approximated as

$$\min_{\mathbf{q}_k^h, \mu_{m,k}, \theta_{m,k}} \sum_{m=1}^{M}\sum_{k=1}^{K} p_m \frac{a_{m,k} D_m}{\mu_{m,k}} \tag{35}$$
$$\text{s.t. (30a), (31a)},$$
$$d_{k,j}^{h,lb} \ge D^h, \forall k \in \mathcal{K}, j \ne k, \tag{35a}$$
$$\mu_{m,k} \le \hat{R}_{m,k}^{lb}, \forall m \in \mathcal{M}, \forall k \in \mathcal{K}, \tag{35b}$$
$$\theta_{m,k} \le Q_{m,k}^r - O_{m,k}^r(d_{m,k} - d_{m,k}^r),$$
$$\forall m \in \mathcal{M}, \forall k \in \mathcal{K}. \tag{35c}$$

Since the objective function and the constraints are all convex, problem (35) is a convex optimization problem. Therefore, the solution can be obtained by the interior-point method.

2) Vertical coordinate optimization problem: Given any feasible horizontal coordinate x_k and y_k, problem (29) is transformed into

$$\min_{z_u} \sum_{m=1}^{M}\sum_{k=1}^{K} \hat{E}_{m,k}^{O} \tag{36}$$
$$\text{s.t. (19a)},$$
$$z_{min} \le z_k \le z_{max}, \forall k \in \mathcal{K}, \tag{36a}$$
$$(z_k - z_j)^2 \ge D^v, \forall k \in \mathcal{K}, j \ne k, \tag{36b}$$

where $D^v = d_{min} - \|\mathbf{q}_k^h - \mathbf{q}_j^h\|^2$ is constant. Note that this problem is similar to problem (30). Hence, a similar approach can be adopted to solve problem (36), i.e., introducing slack variable and applying SCA technique. In this way, given the

Algorithm 1 Overall algorithm for problem (18)

$r \leftarrow 0$
Initialize the offloading strategy $a_{m,k}^r$, the transmit power p_m^r, the frequency bandwidth $B_{m,k}^r$, the computing resource $f_{m,k}^r$, and the hovering locations of the UAVs $\mathbf{q}_k^r$.
repeat
  Solve problem (23) with the local points p_m^r, $B_{m,k}^r$, $f_{m,k}^r$ and $\mathbf{q}_k^r$ by the interior-point method, and obtain the solution $a_{m,k}^*$.
  Update the local point $a_{m,k}^{r+1} \leftarrow a_{m,k}^*$.
  Solve problem (24) with the local points $a_{m,k}^{r+1}$, $B_{m,k}^r$, $f_{m,k}^r$ and $\mathbf{q}_k^r$ by formula (25), and obtain the solution p_m^*.
  Update the local point $p_m^{r+1} \leftarrow p_m^*$.
  Solve problem (26) with the local points $a_{m,k}^{r+1}$, p_m^{r+1}, $f_{m,k}^r$ and $\mathbf{q}_k^r$ by the interior-point method, and obtain the solution $B_{m,k}^*$.
  Update the local point $B_{m,k}^{r+1} \leftarrow B_{m,k}^*$.
  Solve problem (27) with the local points $a_{m,k}^{r+1}$, p_m^{r+1}, $B_{m,k}^{r+1}$ and $\mathbf{q}_k^r$ by formula (28), and obtain the solution $f_{m,k}^*$.
  Update the local point $f_{m,k}^{r+1} \leftarrow f_{m,k}^*$.
  Solve problem (29) with the local points $a_{m,k}^{r+1}$, p_m^{r+1}, $B_{m,k}^{r+1}$ and $f_{m,k}^{r+1}$ by solving problems (35) and (37), and obtain the solution $\mathbf{q}_k^*$.
  Update the local point $\mathbf{q}_k^{r+1} \leftarrow \mathbf{q}_k^*$.
  $r \leftarrow r+1$.
until The objective value converges.

local points z_k^r and $\phi_{m,k}^r$ in the r-th iteration, problem (36) can be transformed into

$$\min_{z_k,\nu_{m,k},\phi_{m,k}} \sum_{m=1}^{M}\sum_{k=1}^{K} p_m \frac{a_{m,k}D_m}{\nu_{m,k}} \tag{37}$$

s.t. (36a),

$$-(z_k^r - z_j^r)^2 + 2(z_k^r - z_j^r)(z_k - z_j) \geq D^z, \quad \forall k \in \mathcal{K}, j \neq k, \tag{37a}$$

$$\frac{a_{m,k}D_m}{\nu_{m,k}} \leq S_m, \forall m \in \mathcal{M}, \forall k \in \mathcal{K}, \tag{37b}$$

$$\nu_{m,k} \leq \tilde{R}_{m,k}^{lb}, \forall m \in \mathcal{M}, \forall k \in \mathcal{K}, \tag{37c}$$

$$\phi_{m,k} \leq \frac{180}{\pi}\arcsin(\frac{z_k}{d_{m,k}}), \quad \forall m \in \mathcal{M}, \forall k \in \mathcal{K}, \tag{37d}$$

where the LHS of the inequality in constraint (37a) is the lower bound of that in constraint (36b) at the given z_k^r, and $\tilde{R}_{m,k}^{lb}$ is the lower bound of $\hat{R}_m$ at the given z_k^r and $\phi_{m,k}^r$. They are obtained by the SCA technique similar to formula (32) and (33), respectively. In this problem, the objective function is convex, constraint (36a) is linear, and the other constraints are convex. Therefore, problem (37) is a convex optimization problem, which can also be solve by the interior-point method.

F. Alternative algorithm

Based on the above solutions, an alternative algorithm is proposed to solve the original problem (18). According to the degree of initialization difficulty, this algorithm first optimizes the offloading strategy $\mathbf{A}$, and then sequentially optimizes the other variables. First, in the $(r+1)$-th iteration, given the transmit power $\mathbf{P}^r$, the frequency bandwidth $\mathbf{B}^r$, computing resource $\mathbf{F}^r$, and hovering location $\mathbf{Q}^r$, problem (23) is solved to obtain the offloading strategy $\mathbf{A}^{r+1}$. Second, with $\mathbf{A}^{r+1}$, $\mathbf{B}^r$, $\mathbf{F}^r$, and $\mathbf{Q}^r$, problem (24) is solved to obtain $\mathbf{P}^{r+1}$ by formula (25). Third, with $\mathbf{A}^{r+1}$, $\mathbf{P}^{r+1}$, $\mathbf{F}^r$, and $\mathbf{Q}^r$, problem (26) is solved to obtained the $\mathbf{B}^{r+1}$ through the interior-point method. Fourth, with $\mathbf{A}^{r+1}$, $\mathbf{P}^{r+1}$, $\mathbf{B}^{r+1}$, and $\mathbf{Q}^r$, problem (27) is solved to obtained the $\mathbf{F}^{r+1}$ through formula (28). Finally, with $\mathbf{A}^{r+1}$, $\mathbf{P}^{r+1}$, $\mathbf{B}^{r+1}$, and $\mathbf{F}^{r+1}$, problem (29) is solved to obtained $\mathbf{Q}^{r+1}$ by optimizing the horizontal and vertical coordinates of the hovering locations, respectively. The iteration continues until the objective value of problem (18) converges. The details of the alternative algorithm is summarized in Algorithm 1.

G. Convergence and Complexity Analysis

It can be verified that the objective value of problem (18) is non-increasing after each iteration of Algorithm 1. Moreover, the objective function of problem (18) is lower-bounded by a finite value. Therefore, the convergence of Algorithm 1 is guaranteed.

Note that the complexity of Algorithm 1 lies in solving the problems (23), (26) and (29). They are solved by the interior-point method. Therefore, their complexities of solving these problems are roughly given by $O(L(2MK)^{3.5})$, $O(L(MK)^{3.5})$ and $O(L((2MK+2K)^{3.5}+(2MK+K)^{3.5}))$, respectively, where L represents the number of iterations. Hence, the complexity of the overall algorithm is $O(L((2MK)^{3.5}+(MK)^{3.5}+(2MK+2K)^{3.5}+(2MK+K)^{3.5}))$.

IV. Simulation Results

In this section, numerical results are provided to validate the effectiveness of the proposed algorithm. We consider the AoI-aware UAV-aided MEC system with $M = 10$ IoT devices that are randomly and uniformly distributed within a square area of 1×1 km^2. For ease of analysis, the IoT devices are assumed to be the same, i.e., they have the same parameters: the task generation rate of each device is set as $\lambda_m = 1$; the APAoI requirement of each device is set as $\tau_m = 50$ s; the data size of the computing task generated by each device is set as $D_m = 10$ Kbits; the required number of CPU cycles for executing 1 bit task is set as $C_m = 1000$ cycle/bit; the maximum transmit power of each device is set as $P_{max} = 0.1$ W. Then, the vertical coordinate range of the UAV hovering location is set as $[30, 100]$ m. The number of UAV is set as $K = 3$. The maximum channel bandwidth and CPU frequency of each UAV are set as $B_{max} = 20$ MHz and $f_{max} = 10$ GHz, respectively. The channel power gain at the reference distance of $d_0 = 1$ m is $\rho_0 = -60$ dB. The LoS and NLoS path loss components are $\alpha_L = 2.5$ and $\alpha_N = 3.5$, respectively.

TABLE I
SIMULATION PARAMETERS

Parameter	Description	Value
M	Number of IoT devices	10
K	Number of UAVs	3
λ_m	Task generation rate	1
D_m	Computing data size	10 Kbits
τ_m	APAoI requirement	50 s
C_m	Required CPU cycles for executing 1 bit data	1000 cycle/bit
P_{max}	Maximum transmit power	0.1 W
B_{max}	Maximum channel bandwidth	20 MHz
f_{max}	Maximum CPU frequency	10 GHz
ρ_0	Channel power gain at the reference distance of 1m	-60 dB
α_L	LoS path loss component	2.5
α_N	NLoS path loss component	3.5
a	Environment parameter	11.95
b	Environment parameter	0.14
N_0	Noise power spectral density	-169 dBm/Hz
η	Efficient switched capacitance	10^{-26}
ϵ	Convergence accuracy	10^{-6}

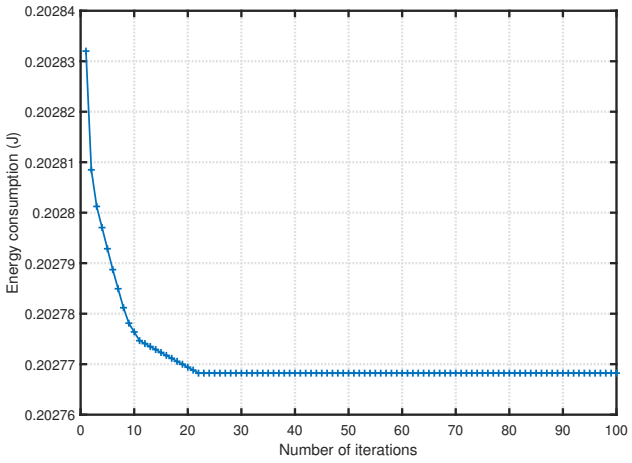

Fig. 4. Convergence of Algorithm 1.

The environment parameters are $a = 11.95$ and $b = 0.14$. The power spectral density of the noise at the receiver is $N_0 = -169$ dBm/Hz. The effective switched capacitance is $\eta = 10^{-26}$. The convergence accuracy of the Algorithm 1 is $\epsilon = 10^{-6}$. Unless otherwise stated, the main simulation parameters are summarized in Table I. For ease of expression, the energy consumption mentioned in this section refers to the energy expended by the UAVs and the IoT devices in processing tasks generated within a unit time.

For analysis, we consider other three algorithms: 1) Maximum transmit power (MTP) algorithm: all the IoT devices offload data at the maximum power; 2) Random hovering location (RHL) algorithm: the UAVs hover at any feasible locations; 3) Equal task assignment (ETA) algorithm: the tasks of each IoT device are equally offloaded to the UAVs.

First, the convergence of the proposed algorithm is shown in Fig. 4. It can be observed that the objective value decreases quickly and the proposed algorithm can converges in a few iterations. This demonstrates the convergence analysis in Section III-G.

For ease of expression, we define the energy minimization schemes with AoI and latency constraints as Scheme I and Scheme II, respectively. The average APAoI of the IoT devices in these schemes is plotted in Fig. 5. It can be observed that the average APAoI of Scheme I consistently meets the APAoI requirements of the IoT devices, and is lower than that of the Scheme II. The reason is that Scheme I needs to minimize the energy consumption while considering the APAoI requirements of the IoT devices. By contrast, Scheme II minimizes the energy consumption just considering the average latency of the tasks offloaded by the IoT devices, which results in large APAoI of the devices. Moreover, one can also see from Fig. 5 that the average APAoI decreases with the increase in the maximum frequency bandwidth and the number of UAVs, but increases as the other parameters increase. That is because more bandwidth and UAVs results in more communication and computing resources, but more data size, task generation rate and number of IoT devices results in more workload. With more resources, these schemes can reduce the APAoI of the devices by reasonably allocating the resource. However, with more workload, limited resource increases the APAoI of the devices.

Then, we also simulate the energy consumption under these schemes. However, the difference in energy consumption between Scheme I and Scheme II is marginal. To illustrate the performance of these schemes clearly, we only present some representative results in Fig. 6. Notably, the energy consumption in Scheme I and Scheme II appears proximate. However, Scheme I demonstrates slightly higher energy consumption. Consequently, in Scheme I, the IoT devices achieve a lower APAoI while the system consumes similar energy with that in Scheme II.

To demonstrate the analysis of the bandwidth allocation in Remark 1 of Section III-C, we simulate the proposed algorithm with respect to the maximum frequency bandwidth of each UAV under different APAoI requirements. The results are depicted in Fig. 7. As can be seen, the energy consumption decreases as the maximum bandwidth increases, and the rate of decrease progressively diminishes. This is consistent with the analysis in Remark 1. Since all the bandwidth is allocated to the IoT devices, the bandwidth allocated to each device increases with the increase in the maximum bandwidth. This reduces the offloading duration, and thus decreasing the energy consumption. However, the impact of the bandwidth on the energy consumption is limited. As the maximum bandwidth continuously increases, the energy consumption gradually approaches a constant value. Moreover, it can be also observed from Fig. 7 that the energy consumption of the system with low APAoI tolerance is larger than that of the system with high APAoI tolerance, and the system with low APAoI tolerance exhibits a slower convergence of energy consumption. The reason is that the system with low APAoI tolerance needs more resource to meet the APAoI requirements of the IoT devices, which increases the energy consumption. Furthermore, more

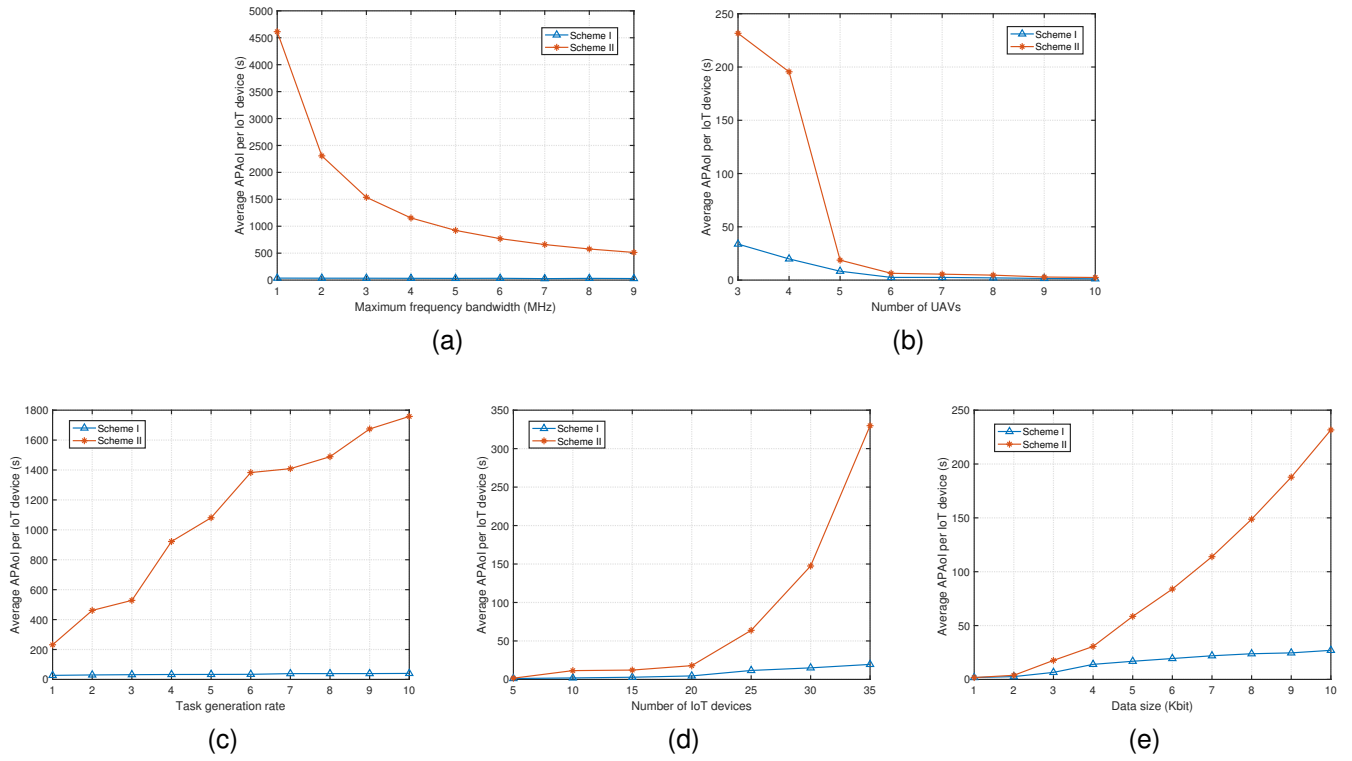

Fig. 5. Comparison of average APAoI in different schemes. (a) Maximum Ffequency bandwidth B_{max}. (b) Number of UAVs K. (c) Task generation rate λ_m. (d) Number of IoT devices M. (e) Data size of tasks D_m.

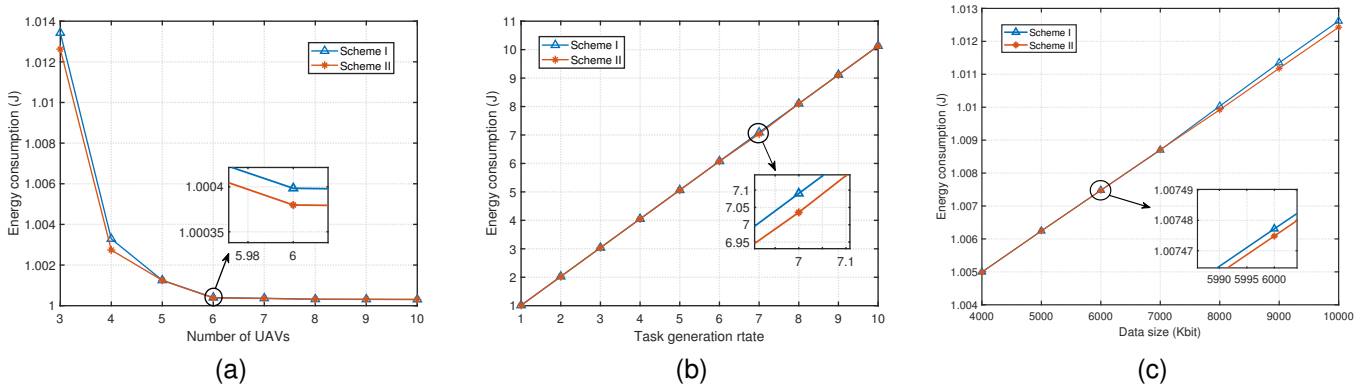

Fig. 6. Comparison of energy consumption in different schemes. (a) Number of UAVs K. (b) Task generation rate λ_m. (c) Data size of tasks D_m.

allocated resource (i.e., the transmit power) leads to the increase in the numerator of the energy consumption $\hat{E}^O_{m,k}$ for offloading, thereby decelerating the convergence of the energy consumption.

To valid the effectiveness of the proposed algorithm, we compare it with three other algorithms in Fig. 8. Similar to Fig. 5, the energy consumption increases as the data size and the number of IoT devices increase. This is due to the increased demand for communication and computing resources. Furthermore, from Fig. 8(b), one can see that the increase rate of energy consumption first increases and then decreases with respect to the number of IoT devices. This is because that the system needs to consume more energy to process the additional tasks generated by the extra devices. However, as the number of devices continues to increase, the computing resource is gradually being fully utilized. The further increase of the number of devices can only results in a small increase in the energy consumption. In Fig. 8(c), the energy consumption obtained by the proposed, the MTP and the RHL algorithms decreases as the number of UAV increases, but the decrease rate progressively diminishes. The reason is that the increase in the number of the UAVs implies the increase in the network resource, and then the tasks of the IoT devices can be assigned more properly to reduce the energy consumption while satisfying the their APAoI requirements. However, the resource demand of the system has

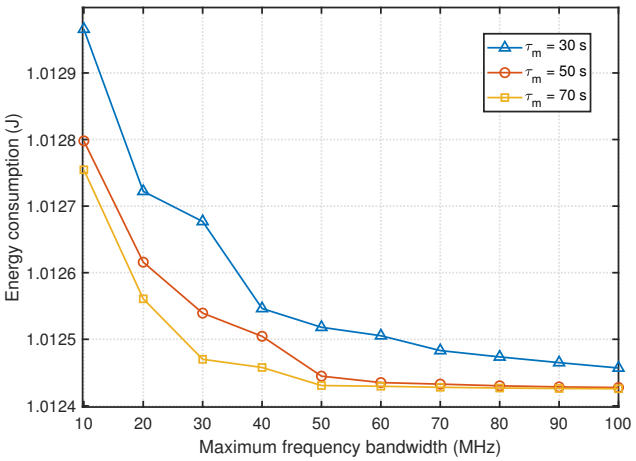

Fig. 7. Energy consumption versus maximum frequency bandwidth.

an upper bound. When the resource of the UAVs reaches the bound, additional resource becomes redundant. Therefore, the decrease rate of the energy consumption gradually decelerates. As for the ETA algorithm, the energy consumption increases with respect to the number of UAVs. That is because the tasks are assigned equally to the UAVs. The increase in the number of UAVs may paradoxically reduce the rationality of the offloading strategy.

Compared with other algorithms, it can also be observed that the proposed algorithm achieves the best performance in Fig. 8, since all the resources are optimized in it. In contrast, the IoT devices always offload at the maximum power in the MTP algorithm. Although maximum transmit power reduces the offloading duration, it generates excessive transmission consumption for the devices close to the connected UAV. As for the RHL algorithm, the stationary UAVs are equivalent to the BSs. They can not provide large transmit rate for the far devices, and thus increasing the energy consumption of transmission. Furthermore, these devices need more computing resource to meet their APAoI requirement, thereby increasing the computing consumption. Finally, due to the equal task assignment, the ETA algorithm can not allocate the resource of the UAVs properly to the IoT devices. Therefore, these algorithms perform worse than the proposed algorithm.

V. Conclusion

In this paper, we have investigated the AoI-aware UAV-aided MEC system, where the UAVs provide computing service for the ground IoT devices with heterogeneous APAoI requirements. Based on the Poisson process model, the probabilistic LoS channel model and the M/D/1 queue model, we have derived the mathematical expression of the APAoI for each IoT device. It consists of four parts: task generation interval and the duration of transmission, waiting, and computing. Then, we have formulated the optimization problem to minimize the energy consumption of the system for executing the tasks generated in unit time by jointly optimizing the offloading strategy and the transmit power of the devices, and the bandwidth and computing resource allocation as well as the hovering locations of the UAVs, subject to the APAoI, hovering location, communication and computing constraints. This is a non-convex problem, and thus being challenging to solve. As such, to solve the original problem efficiently, we have decomposed it into five suproblems and proposed an iterative algorithm to alternatively solve these subproblems, based on the traditional mathematical method, the KKT conditions, and the SCA technique. Numerical results have shown that the energy minimization scheme with APAoI constraint has advantages, and the proposed algorithm can reduce the energy consumption compared to the benchmark algorithms.

Appendix A
Proof of Lemma 1

Define $f(x) = \log_2(1+x) - \frac{x}{\ln 2(1+x)}$. The first-order derivative of $f(x)$ is given by $f'(x) = \frac{x}{\ln 2(1+x)^2}$. Note that $f'(x) \geq 0$ for $x \geq 0$. Therefore, $f(x)$ is a monotonically increasing function for $x \geq 0$. Since $f(0) = 0$, one can have $f(x) \geq 0$ for $x \geq 0$.

Then, let $\Omega = \sum_{m=1}^{M}\sum_{k=1}^{K} \hat{E}^O_{m,k}$. The first-order derivatives of Ω with respect to p_m is given by

$$\frac{\partial \Omega}{\partial p_m} = \sum_{k=1}^{K} \frac{\log_2(1+X_{m,k}p_m) - \frac{X_{m,k}p_m}{\ln 2(1+X_{m,k}p_m)}}{U_{m,k}[\log_2(1+X_{m,k}p_m)]^2}, \quad (38)$$

where $U_{m,k} = \frac{B_{m,k}P^{LoS}_{m,k}}{a_{m,k}D_m}$ and $X_{m,k} = \frac{\gamma}{B_{m,k}d^{\alpha_L}_{m,k}}$ are non-negative constants.

Let $X_{m,k}p_m = t$, then the numerator of the RHS of the equality in (38) can be transformed into $g(t) = \log_2(1+t) - \frac{t}{\ln 2(1+t)}$. According to the previous proof, we have $g(t) \geq 0$ for $t \geq 0$. Thus, $\frac{\partial \Omega}{\partial p_m} \geq 0$ for $p_m \geq 0$. Therefore, Ω is monotonically increasing with respect to p_m. The proof is completed.

Appendix B
Proof of Remark 1

Define $\Phi(x) = x\log_2(1+\frac{C_1}{x})$ with C_1 being a positive constant. The first-order and second-order derivatives of $\Phi(x)$ are respectively given by

$$\Phi'(x) = \log_2(1+\frac{C_1}{x}) - \frac{C_1}{(x+C_1)\ln 2}, \quad (39)$$

$$\Phi''(x) = -\frac{C_1^2}{x(x+C_1)^2\ln 2}. \quad (40)$$

Since $\Phi''(x) \geq 0$ for $x \geq 0$, $\Phi'(x)$ is a monotonically increasing function for $x \geq 0$. Moreover, $\lim_{x\to\infty} \Phi'(x) = 0$. Hence, we have $\Phi'(x) \geq 0$ for $x \geq 0$, and thus $\Phi(x)$ is a monotonically increasing function for $x \geq 0$.

The objective function and the offloading duration can be transformed into $\hat{E}^O_{m,k} = \frac{C_2}{B_{m,k}\log_2(1+\frac{C_3}{B_{m,k}})}$ and $\hat{T}^O_{m,k} = \frac{C_4}{B_{m,k}\log_2(1+\frac{C_3}{B_{m,k}})}$, respectively, with $C_2 = \frac{a_{m,k}p_mD_m}{P^{LoS}_{m,k}}$, $C_3 = \frac{p_m\gamma}{d^{\alpha_L}_{m,k}}$ and $C_4 = \frac{a_{m,k}D_m}{P^{LoS}_{m,k}}$ being positive constants. Therefore, $\hat{E}^O_{m,k}$ and $\hat{T}^O_{m,k}$ are both monotonically decreasing function with respect to $B_{m,k}$ for $B_{m,k} \geq 0$. Furthermore, since

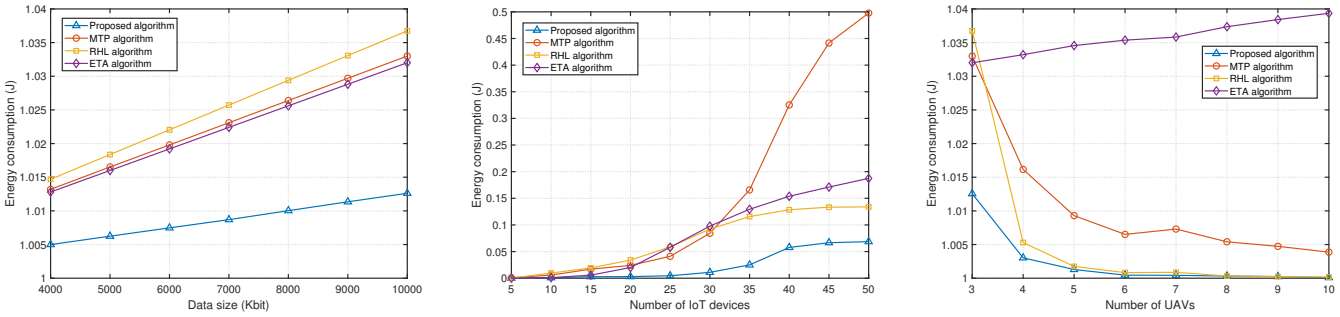

Fig. 8. Comparison of energy consumption in different algorithms. (a) Data size of tasks D_m. (b) Number of IoT devices M. (c) Number of UAVs K.

$\lim_{B_{m,k}\to\infty} \hat{E}^O_{m,k} = \frac{C_2(1+\frac{C_3}{B_{m,k}})\ln 2}{C_3}$, the energy consumption gradually decreases and converges to a constant. That is to say, the energy consumption gradually decreases to an asymptotic constant with respect to $B_{m,k}$. Therefore, to minimize the energy consumption, the bandwidth of each UAV is all allocated to the IoT devices. The proof is completed.

Appendix C
Proof of the Solution of Problem (27)

The Lagrangian of problem (27) can be given by

$$\begin{aligned}
&L_2(\mathbf{F},\boldsymbol{\nu},\boldsymbol{\omega},\boldsymbol{\varphi})\\
&=\sum_{m=1}^{M}\sum_{k=1}^{K}E^C_{m,k}+\sum_{k=1}^{K}\nu_k\Big(\sum_{m=1}^{M}f_{m,k}-f_{max}\Big)\\
&+\sum_{m=1}^{M}\sum_{k=1}^{K}\varphi_{m,k}\Big(\frac{\lambda_m}{2\frac{f_{m,k}}{a_{m,k}F_m}\big(\frac{f_{m,k}}{a_{m,k}F_m}-\lambda_m\big)}+\frac{a_{m,k}F_m}{f_{m,k}}-J_{m,k}\Big)\\
&+\sum_{m=1}^{M}\sum_{k=1}^{K}\omega_{m,k}(\lambda_m a_{m,k}F_m-f_{m,k}),
\end{aligned}\tag{41}$$

where ν_k, $\varphi_{m,k}$ and $\omega_{m,k}$ are the nonnegative Lagrange multipliers. Then, the KKT conditions can be expressed as

$$\begin{aligned}
&\varphi_{m,k}\Big(\frac{\lambda_m}{2}\cdot\frac{\frac{\lambda_m}{a_{m,k}F_m}-\frac{2}{a^2_{m,k}F^2_m}f_{m,k}}{\big[\frac{f_{m,k}}{a_{m,k}F_m}\big(\frac{f_{m,k}}{a_{m,k}F_m}-\lambda_m\big)\big]^2}-\frac{a_{m,k}F_m}{f^2_{m,k}}\Big)\\
&+2\mu a_{m,k}F_m f_{m,k}+\nu_k-\omega_{m,k}=0,\forall m\in\mathcal{M},\forall k\in\mathcal{K},
\end{aligned}\tag{42}$$

$$\nu_k\Big(\sum_{m=1}^{M}f_{m,k}-f_{max}\Big)=0,\forall k\in\mathcal{K},\tag{43}$$

$$\begin{aligned}
&\varphi_{m,k}\Big(\frac{\lambda_m}{2\frac{f_{m,k}}{a_{m,k}F_m}\big(\frac{f_{m,k}}{a_{m,k}F_m}-\lambda_m\big)}+\frac{a_{m,k}F_m}{f_{m,k}}-J_{m,k}\Big)=0,\\
&\forall m\in\mathcal{M},\forall k\in\mathcal{K},
\end{aligned}\tag{44}$$

$$\omega_{m,k}(\lambda_m F_m a_{m,k}-f_{m,k})=0,\forall m\in\mathcal{M},\forall k\in\mathcal{K},\tag{45}$$

$$\sum_{m=1}^{M}f_{m,k}-f_{max}\le 0,\forall k\in\mathcal{K},\tag{46}$$

$$\lambda_m F_m a_{m,k}-f_{m,k}\le 0,\forall m\in\mathcal{M},\forall k\in\mathcal{K},\tag{47}$$

$$\begin{aligned}
&\frac{\lambda_m}{2\frac{f_{m,k}}{a_{m,k}F_m}\big(\frac{f_{m,k}}{a_{m,k}F_m}-\lambda_m\big)}+\frac{a_{m,k}F_m}{f_{m,k}}-J_{m,k}\le 0,\\
&\forall m\in\mathcal{M},\forall k\in\mathcal{K},
\end{aligned}\tag{48}$$

$$f_{m,k}\ge 0,\nu_k\ge 0,\omega_{m,k}\ge 0,\varphi_{m,k}\ge 0,\forall m\in\mathcal{M},\forall k\in\mathcal{K}.\tag{49}$$

From (48), we have $\lambda_m F_m a_{m,k}-f_{m,k}\neq 0$. Thus, according to (45), one can have $\omega_m=0$. Moreover, it can be verified that the first term of (42) is negative. In order to guarantee that the equality of (42) holds, $\varphi_{m,k}$ can not equal to zero, i.e., $\varphi_{m,k}\neq 0$. Therefore, we have $\frac{\lambda_m}{2\frac{f_{m,k}}{a_{m,k}F_m}\big(\frac{f_{m,k}}{a_{m,k}F_m}-\lambda_m\big)}+\frac{a_{m,k}F_m}{f_{m,k}}-J_{m,k}=0$ from (44), which can be transformed into

$$-\frac{2J_{m,k}}{a^2_{m,k}F^2_m}f^2_{m,k}+\frac{2(J_{m,k}\lambda_m+1)}{a_{m,k}F_m}f_{m,k}-\lambda_m=0.\tag{50}$$

Then, $f_{m,k}$ can be obtained as

$$f_{m,k}=\frac{[(J_{m,k}\lambda_m+1)+\sqrt{J^2_{m,k}\lambda^2_m+1}]a_{m,k}F_m}{2J_{m,k}},\tag{51}$$

or

$$f_{m,k}=\frac{[(J_{m,k}\lambda_m+1)-\sqrt{J^2_{m,k}\lambda^2_m+1}]a_{m,k}F_m}{2J_{m,k}}.\tag{52}$$

Since $J_{m,k}\lambda_m\ge 0$, we have $\sqrt{J^2_{m,k}\lambda^2_m+1}\ge 1$. Then, for (52), one can have

$$\begin{aligned}
f_{m,k}&=\frac{[(J_{m,k}\lambda_m+1)-\sqrt{J^2_{m,k}\lambda^2_m+1}]a_{m,k}F_m}{2J_{m,k}}\\
&\le\frac{\lambda_m F_m a_{m,k}}{2},
\end{aligned}\tag{53}$$

which contradicts (47). Therefore, the optimal solution of problem (27) can be expressed as

$$f^*_{m,k}=\frac{[(J_{m,k}\lambda_m+1)+\sqrt{J^2_{m,k}\lambda^2_m+1}]a_{m,k}F_m}{2J_{m,k}}.\tag{54}$$

The proof is completed.

APPENDIX D
PROOF OF THE LEMMA 2

The second-order partial derivatives of $\psi(t_1, t_2)$ are given by

$$\frac{\partial^2 \psi(t_1,t_2)}{\partial t_1^2} = \frac{2A_1}{\ln 2 t_1^3} \ln(1+\frac{A_2}{t_2}), \tag{55}$$

$$\frac{\partial^2 \psi(t_1,t_2)}{\partial t_2^2} = \frac{A_1 A_2 t_2^{-3}(2+A_2 t_2^{-1})}{\ln 2 t_1 (1+A_2 t_2^{-1})^2}, \tag{56}$$

$$\frac{\partial^2 \psi(t_1,t_2)}{\partial t_1 t_2} = \frac{\partial^2 \psi(t_1,t_2)}{\partial t_2 t_1} = \frac{A_1 A_2 t_2^{-2}}{\ln 2 t_1^2 (1+A_2 t_2^{-1})}. \tag{57}$$

One can see that $\frac{\partial^2 \psi(t_1,t_2)}{\partial t_1^2} > 0$ for $t_1 > 0$ and $t_2 > 0$. Moreover, we have

$$\begin{aligned}
&\frac{\partial^2 \psi(t_1,t_2)}{\partial t_1^2}\frac{\partial^2 \psi(t_1,t_2)}{\partial t_2^2} - \frac{\partial^2 \psi(t_1,t_2)}{\partial t_1 t_2}\frac{\partial^2 \psi(t_1,t_2)}{\partial t_2 t_1} \\
&= \frac{2A_1^2 A_2 t_2^{-3}(2+A_2 t_2^{-1})\ln(1+\frac{A_2}{t_2}) - A_1^2 A_2^2 t_2^{-4}}{(\ln 2)^2 t_1^4 (1+A_2 t_2^{-1})^2} \\
&\overset{(a)}{\geq} \frac{A_1^2 A_2 t_2^{-3}}{(\ln 2)^2 t_1^4 (1+A_2 t_2^{-1})^2} \cdot \frac{3+A_2 t_2^{-1}}{t_2 + B} > 0,
\end{aligned} \tag{58}$$

where (a) is due to $\ln(1+\frac{1}{t_3}) \geq \frac{1}{t_3+1}$ for $t_3 > 0$. Therefore, the Hessian matrix of $\psi(t_1, t_2)$ is positive definite. Thus, $\psi(t_1, t_2)$ is a convex function. The proof is completed.

REFERENCES

[1] K. Wang, K. Yang, and C. S. Magurawalage, "Joint energy minimization and resource allocation in C-RAN with mobile cloud," *IEEE Transactions on Cloud Computing*, vol. 6, no. 3, pp. 760–770, 2018.

[2] Y. Mao, C. You, J. Zhang, K. Huang, and K. B. Letaief, "A survey on mobile edge computing: The communication perspective," *IEEE Communications Surveys & Tutorials*, vol. 19, no. 4, pp. 2322–2358, 2017.

[3] M. Li, N. Cheng, J. Gao, Y. Wang, L. Zhao, and X. Shen, "Energy-efficient UAV-assisted mobile edge computing: Resource allocation and trajectory optimization," *IEEE Transactions on Vehicular Technology*, vol. 69, no. 3, pp. 3424–3438, 2020.

[4] Z. Yang, S. Bi, and Y.-J. A. Zhang, "Online trajectory and resource optimization for stochastic UAV-enabled MEC systems," *IEEE Transactions on Wireless Communications*, vol. 21, no. 7, pp. 5629–5643, 2022.

[5] Y. Zeng, R. Zhang, and T. J. Lim, "Wireless communications with unmanned aerial vehicles: opportunities and challenges," *IEEE Communications Magazine*, vol. 54, no. 5, pp. 36–42, 2016.

[6] Y. Zheng, J. Hu, and K. Yang, "Average age of information in wireless powered relay aided communication network," *IEEE Internet of Things Journal*, vol. 9, no. 13, pp. 11 311–11 323, 2022.

[7] A. Muhammad, I. Sorkhoh, M. Samir, D. Ebrahimi, and C. Assi, "Minimizing age of information in multi-access edge computing-assisted IoT networks," *IEEE Internet of Things Journal*, 2021.

[8] R. D. Yates and S. K. Kaul, "The age of information: Real-time status updating by multiple sources," *IEEE Transactions on Information Theory*, vol. 65, no. 3, pp. 1807–1827, 2019.

[9] W. Wu, F. Zhou, R. Q. Hu, and B. Wang, "Energy-efficient resource allocation for secure NOMA-enabled mobile edge computing networks," *IEEE Transactions on Communications*, vol. 68, no. 1, pp. 493–505, 2020.

[10] W. Zhang, G. Zhang, and S. Mao, "Joint parallel offloading and load balancing for cooperative-MEC systems with delay constraints," *IEEE Transactions on Vehicular Technology*, vol. 71, no. 4, pp. 4249–4263, 2022.

[11] K. Guo, R. Gao, W. Xia, and T. Q. S. Quek, "Online learning based computation offloading in MEC systems with communication and computation dynamics," *IEEE Transactions on Communications*, vol. 69, no. 2, pp. 1147–1162, 2021.

[12] Y. Liu, J. Liu, A. Argyriou, L. Wang, and Z. Xu, "Rendering-aware VR video caching over multi-cell MEC networks," *IEEE Transactions on Vehicular Technology*, vol. 70, no. 3, pp. 2728–2742, 2021.

[13] Z. Xiao, X. Dai, H. Jiang, D. Wang, H. Chen, L. Yang, and F. Zeng, "Vehicular task offloading via heat-aware MEC cooperation using game-theoretic method," *IEEE Internet of Things Journal*, vol. 7, no. 3, pp. 2038–2052, 2020.

[14] S. D. A. Shah, M. A. Gregory, S. Li, R. d. R. Fontes, and L. Hou, "SDN-based service mobility management in MEC-enabled 5G and beyond vehicular networks," *IEEE Internet of Things Journal*, vol. 9, no. 15, pp. 13 425–13 442, 2022.

[15] L. Shi, Y. Ye, X. Chu, and G. Lu, "Computation energy efficiency maximization for a NOMA-based WPT-MEC network," *IEEE Internet of Things Journal*, vol. 8, no. 13, pp. 10 731–10 744, 2021.

[16] R. Malik and M. Vu, "Energy-efficient joint wireless charging and computation offloading in MEC systems," *IEEE Journal of Selected Topics in Signal Processing*, vol. 15, no. 5, pp. 1110–1126, 2021.

[17] Z. Ding, D. Xu, R. Schober, and H. V. Poor, "Hybrid NOMA offloading in multi-user MEC networks," *IEEE Transactions on Wireless Communications*, vol. 21, no. 7, pp. 5377–5391, 2022.

[18] F. Pervez, A. Sultana, C. Yang, and L. Zhao, "Energy and latency efficient joint communication and computation optimization in a multi-UAV assisted MEC network," *IEEE Transactions on Wireless Communications*, pp. 1–1, 2023.

[19] W. Mao, K. Xiong, Y. Lu, P. Fan, and Z. Ding, "Energy consumption minimization in secure multi-antenna UAV-assisted MEC networks with channel uncertainty," *IEEE Transactions on Wireless Communications*, pp. 1–1, 2023.

[20] B. Dai, J. Niu, T. Ren, Z. Hu, and M. Atiquzzaman, "Towards energy-efficient scheduling of UAV and base station hybrid enabled mobile edge computing," *IEEE Transactions on Vehicular Technology*, vol. 71, no. 1, pp. 915–930, 2022.

[21] X. Hu, K.-K. Wong, and Y. Zhang, "Wireless-powered edge computing with cooperative uav: Task, time scheduling and trajectory design," *IEEE Transactions on Wireless Communications*, vol. 19, no. 12, pp. 8083–8098, 2020.

[22] Q. Zhang, J. Chen, L. Ji, Z. Feng, Z. Han, and Z. Chen, "Response delay optimization in mobile edge computing enabled UAV swarm," *IEEE Transactions on Vehicular Technology*, vol. 69, no. 3, pp. 3280–3295, 2020.

[23] Y. Liu, J. Yan, and X. Zhao, "Deep reinforcement learning based latency minimization for mobile edge computing with virtualization in maritime UAV communication network," *IEEE Transactions on Vehicular Technology*, vol. 71, no. 4, pp. 4225–4236, 2022.

[24] Y. Xu, T. Zhang, J. Loo, D. Yang, and L. Xiao, "Completion time minimization for UAV-assisted mobile-edge computing systems," *IEEE Transactions on Vehicular Technology*, vol. 70, no. 11, pp. 12 253–12 259, 2021.

[25] E. E. Haber, H. A. Alameddine, C. Assi, and S. Sharafeddine, "UAV-aided ultra-reliable low-latency computation offloading in future IoT networks," *IEEE Transactions on Communications*, vol. 69, no. 10, pp. 6838–6851, 2021.

[26] M. K. Abdel-Aziz, S. Samarakoon, C.-F. Liu, M. Bennis, and W. Saad, "Optimized age of information tail for ultra-reliable low-latency communications in vehicular networks," *IEEE Transactions on Communications*, vol. 68, no. 3, pp. 1911–1924, 2020.

[27] S. Zhang, J. Li, H. Luo, J. Gao, L. Zhao, and X. Sherman Shen, "Low-latency and fresh content provision in information-centric vehicular networks," *IEEE Transactions on Mobile Computing*, vol. 21, no. 5, pp. 1723–1738, 2022.

[28] A. Arafa, J. Yang, S. Ulukus, and H. V. Poor, "Age-minimal transmission for energy harvesting sensors with finite batteries: Online policies," *IEEE Transactions on Information Theory*, vol. 66, no. 1, pp. 534–556, 2020.

[29] H. Zheng, K. Xiong, P. Fan, Z. Zhong, and K. B. Letaief, "Age of information-based wireless powered communication networks with selfish charging nodes," *IEEE Journal on Selected Areas in Communications*, vol. 39, no. 5, pp. 1393–1411, 2021.

[30] J. Liu, P. Tong, X. Wang, B. Bai, and H. Dai, "UAV-aided data collection for information freshness in wireless sensor networks," *IEEE Transactions on Wireless Communications*, vol. 20, no. 4, pp. 2368–2382, 2021.

[31] H. Hu, K. Xiong, G. Qu, Q. Ni, P. Fan, and K. B. Letaief, "AoI-minimal trajectory planning and data collection in UAV-assisted wireless powered IoT networks," *IEEE Internet of Things Journal*, vol. 8, no. 2, pp. 1211–1223, 2021.

[32] Z. Ning, P. Dong, X. Wang, X. Hu, L. Guo, B. Hu, Y. Guo, T. Qiu, and R. Y. K. Kwok, "Mobile edge computing enabled 5G health monitoring

for internet of medical things: A decentralized game theoretic approach," *IEEE Journal on Selected Areas in Communications*, vol. 39, no. 2, pp. 463–478, 2021.
[33] L. Liu, X. Qin, X. Xu, H. Li, F. R. Yu, and P. Zhang, "Optimizing information freshness in MEC-assisted status update systems with heterogeneous energy harvesting devices," *IEEE Internet of Things Journal*, vol. 8, no. 23, pp. 17 057–17 070, 2021.
[34] Q. Wu, Z. Wan, Q. Fan, P. Fan, and J. Wang, "Velocity-adaptive access scheme for MEC-assisted platooning networks: Access fairness via data freshness," *IEEE Internet of Things Journal*, vol. 9, no. 6, pp. 4229–4244, 2022.
[35] Z. Qin, Z. Wei, Y. Qu, F. Zhou, H. Wang, D. W. K. Ng, and C.-B. Chae, "AoI-aware scheduling for air-ground collaborative mobile edge computing," *IEEE Transactions on Wireless Communications*, pp. 1–1, 2022.
[36] W. Wang, G. Srivastava, J. C.-W. Lin, Y. Yang, M. Alazab, and T. R. Gadekallu, "Data freshness optimization under CAA in the UAV-aided MECN: A potential game perspective," *IEEE Transactions on Intelligent Transportation Systems*, pp. 1–10, 2022.
[37] R. Han, Y. Wen, L. Bai, J. Liu, and J. Choi, "Age of information aware UAV deployment for intelligent transportation systems," *IEEE Transactions on Intelligent Transportation Systems*, vol. 23, no. 3, pp. 2705–2715, 2022.
[38] A. Al-Hourani, S. Kandeepan, and S. Lardner, "Optimal LAP altitude for maximum coverage," *IEEE Wireless Communications Letters*, vol. 3, no. 6, pp. 569–572, 2014.
[39] Y. Zeng, J. Xu, and R. Zhang, "Energy minimization for wireless communication with rotary-wing UAV," *IEEE Transactions on Wireless Communications*, vol. 18, no. 4, pp. 2329–2345, 2019.
[40] Y. Mao, C. You, J. Zhang, K. Huang, and K. B. Letaief, "A survey on mobile edge computing: The communication perspective," *IEEE Communications Surveys Tutorials*, vol. 19, no. 4, pp. 2322–2358, 2017.
[41] C. You and R. Zhang, "Hybrid offline-online design for UAV-enabled data harvesting in probabilistic LoS channels," *IEEE Transactions on Wireless Communications*, vol. 19, no. 6, pp. 3753–3768, 2020.

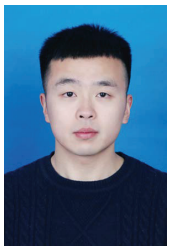

Shuai Shen received his M.S. degree from the School of Information and Control Engineering of China University of Mining and Technology, Xuzhou, China, in 2019. He is currently pursuing the Ph.D. degree in the School of Information and Communication Engineering, University of Electronic Science and Technology of China, Chengdu, China. His research interests include resource efficiency of wireless communications, unmanned aerial vehicle communications and multi-access edge computing.

Halvin Yang received the B.Eng. degree in Electronic and Electrical Engineering from Imperial College London in 2020. He is currently doing a PhD degree for Electronic and Electrical Engineering in University College London starting in 2020. His research interests include resource allocation for edge communications and performance analysis of new 6G technologies like intelligent reflective surfaces (IRS) and fluid antenna communication systems (FACS).

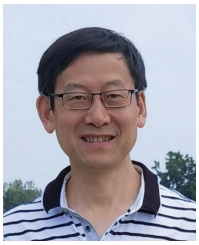

Kun Yang received his PhD from the Department of Electronic & Electrical Engineering of University College London (UCL), UK. He is currently a Chair Professor in the School of Computer Science & Electronic Engineering, University of Essex, UK, leading the Network Convergence Laboratory (NCL). He is also an affiliated professor of Nanjing University, China. His main research interests include wireless networks and communications, future Internet and edge computing. In particular he is interested in energy aspects of future communication systems such as 6G, promoting energy self-sustainability via both energy efficiency (green communications and networks) and energy harvesting (wireless charging). He has managed research projects funded by UK EPSRC, EU FP7/H2020, and industries. He has published 400+ papers and filed 30 patents. He serves on the editorial boards of a number of IEEE journals (e.g., IEEE TNSE, TVT, WCL). He is a Deputy Editor-in-Chief of IET Smart Cities Journal. He has been a Judge of GSMA GLOMO Award at World Mobile Congress – Barcelona since 2019. He was a Distinguished Lecturer of IEEE ComSoc (2020-2021). He is a Member of Academia Europaea (MAE), a Fellow of IEEE, a Fellow of IET and a Distinguished Member of ACM.

Kezhi Wang received the Ph.D. degree from the University of Warwick, U.K. He is a Senior Lecturer with the Department of Computer Science, Brunel University London, U.K. His research interests include wireless communications, mobile edge computing, and machine learning.

Guopeng Zhang received the bachelor's degree from the School of Computer Science, Jiangsu Normal University, Xuzhou, China, in 2001, the master's degree from the School of Computer Science, South China Normal University, Guangzhou, China, in 2005, and the Ph.D. degree from the School of Communication Engineering, Xidian University, Xi'an, China, in 2009. He was with ZTE Corporation Nanjing Branch for one year. In 2009, he joined the China University of Minin and Technology, Xuzhou, China, where he is currently a Professor with the School of Computer Science and Technology. He manages research projects funded by various sources, such as the National Natural Science Foundation of China. He has authored or coauthored more than 60 journal and conference papers. His main research interests include distributed computing and machine learning.